Article ID: 1006-8775(2018) 02-0151-12

A COMPARISON OF THE RETRIEVAL OF ATMOSPHERIC TEMPERATURE PROFILES USING OBSERVATIONS OF THE 60 GHZ AND 118.75 GHZ ABSORPTION LINES

HE Qiu-rui (贺秋瑞)[1, 2], WANG Zhen-zhan (王振占)[1], HE Jie-ying (何杰颖)[1], ZHANG Lan-jie (张兰杰)[1, 2]
(1. Key Laboratory of Microwave Remote Sensing, National Space Science Center, Chinese Academy of Sciences, Beijing 100190 China; 2. University of Chinese Academy of Sciences, Beijing 100049 China)

Abstract: The Microwave Temperature Sounder-II (MWTS-II) and Microwave Humidity and Temperature Sounder (MWHTS) onboard the Fengyun-3C (FY-3C) satellite can be used to detect atmospheric temperature profiles. The MWTS-II has 13 temperature sounding channels around the 60 GHz oxygen absorption band and the MWHTS has 8 temperature sounding channels around the 118.75 GHz oxygen absorption line. The data quality of the observed brightness temperatures can be evaluated using atmospheric temperature retrievals from the MWTS-II and MWHTS observations. Here, the bias characteristics and corrections of the observed brightness temperatures are described. The information contents of observations are calculated, and the retrieved atmospheric temperature profiles are compared using a neural network (NN) retrieval algorithm and a one-dimensional variational inversion (1D-var) retrieval algorithm. The retrieval results from the NN algorithm show that the accuracy of the MWTS-II retrieval is higher than that of the MWHTS retrieval, which is consistent with the results of the radiometric information analysis. The retrieval results from the 1D-var algorithm show that the accuracy of MWTS-II retrieval is similar to that of the MWHTS retrieval at the levels from 850-1,000 hPa, is lower than that of the MWHTS retrieval at the levels from 650-850 hPa and 125-300 hPa, and is higher than that of MWHTS at the other levels. A comparison of the retrieved atmospheric temperature using these satellite observations provides a reference value for assessing the accuracy of atmospheric temperature detection at the 60 GHz oxygen band and 118.75 GHz oxygen line. In addition, based on the comparison of the retrieval results, an optimized combination method is proposed using a branch and bound algorithm for the NN retrieval algorithm, which combines the observations from both the MWTS-II and MWHTS instruments to retrieve the atmospheric temperature profiles. The results show that the optimal combination can further improve the accuracy of MWTS-II retrieval and enhance the detection accuracy of atmospheric temperatures near the surface.

Key words: Fengyun-3C satellite; Microwave Temperature Sounder-II; microwave humidity and temperature sounder; one-dimensional variational retrieval algorithm; neural networks retrieval algorithm

CLC number: P412.27 **Document code:** A

doi: 10.16555/j.1006-8775.2018.02.004

1 INTRODUCTION

Atmospheric temperature profiles play an important role in weather forecasting, climate monitoring, and the analysis of the current weather conditions (Ahn et al.[1]; Stahli et al.[2]). Accurate profiles of temperature may not only be used to assess atmospheric stability and to assist in the nowcasting of intense convective weather but also to initialize and evaluate numerical weather prediction models (Ebell et al.[3]). Microwave remote sensing is an important technique for obtaining atmospheric temperature information. According to microwave spectral theory, microwave absorption and emission by gas molecules in the atmosphere are primarily caused by molecular rotational transitions (Smith[4]; Rosenkranz[5]). Oxygen has a strong absorption band around 60 GHz and an isolated absorption line near 118.75 GHz. Hence, the 60 GHz and 118.75 GHz observations can be used to retrieve atmospheric temperature profiles, since the oxygen concentration in the atmosphere is stable. Currently, the 60 GHz radiometer has reached full development, such as the Microwave Sounding Unit (MSU), the Advanced Microwave Sounding Unit (AMSU)-A, and the Advanced Technology Microwave Sounder (ATMS), with observations widely used in operational applications in the atmosphere (Weng et al.[6]; Ferraro et al.[7]; Boukabara et al.[8]). Compared with the 60 GHz radiometer, the technology of the 118.75 GHz radiometer has developed relatively slowly (Weinman[9]). However, for atmospheric sounding, compared with the 60 GHz oxygen absorption band, there are several advantages of the 118.75 GHz oxygen absorption line, as follows. (1) The simpler superheterodyne radiometers

Received 2017-08-17; **Revised** 2018-02-09; **Accepted** 2018-05-15

Foundation item: Key Fostering Project of the National Space Science Center; Chinese Academy of Sciences (Y62112f37s); National 863 Project of China (2015AA8126027)

Biography: HE Qiu-rui, Ph.D., primarily undertaking research on satellite meteorology.

Corresponding author: WANG Zhen-zhan, e-mail: wangzhen-zhan@mirslab.cn

may be used for sensing, since the 118.75 GHz absorption line is isolated. (2) The oxygen absorption line of 118.75 GHz is advantageous for retrieving atmospheric temperature profiles at altitudes of 50–150 km since it has the simplest Zeeman splitting pattern of all the oxygen absorption lines. (3) For an equivalent antenna diameter, the spatial resolution at 118.75 GHz is half that for 60 GHz. (4) The sensitivity to clouds and precipitation at 118.75 GHz is typically better than that at 60 GHz, and thus the information on clouds and rain may be easier to obtain from observations near the 118.75 GHz absorption line (Gasiewski et al. [10]; Gasiewski et al.[11]; Gasiewski and Johnson[12]). However, because the 118.75 GHz absorption line is more sensitive to clouds, this could in turn affect the retrieval accuracy of atmospheric temperature (Guo et al.[13]).

Comparisons of the retrieval of atmospheric temperature profiles using the 60 GHz and 118 GHz frequencies have been reported, including that by Gasiewski et al [10, 11]. who retrieved atmospheric temperature profiles from airborne observations and carried out sensitivity experiments for water vapor. They concluded that most cloud and precipitation cells are sufficiently transparent for temperature soundings at 118 GHz, although the 118 GHz observations are more sensitive to fluctuations in water vapor density, hydrometeor scattering, and absorption than 60 GHz observations [11]. Sahoo et al. calculated the information content of the simulated brightness temperatures for 118 GHz and 60 GHz, and conducted retrieval experiments of atmospheric temperatures using 118 GHz and 60 GHz simulations to find that the 60 GHz simulations have a higher information content than those at 118 GHz with a higher retrieval accuracy. In addition, they provided an optimized channel combination at 118 GHz and 60 GHz for temperature retrieval [14]. Gu et al. retrieved atmospheric temperature profiles from 54 GHz and 118 GHz simulated brightness temperatures using a statistical retrieval method, with results showing that the simulations of seven channels at 118 GHz can obtain higher retrieval accuracy than those of four channels at 54 GHz [15]. The existing literature on 118 GHz observations contains little research comparing the retrieval of atmospheric temperature profiles using 118 GHz and 60 GHz observations. However, the Fengyun-3C (FY-3C) satellite carrying the Microwave Temperature Sounder-II (MWTS-II) and Microwave Humidity and Temperature Sounder (MWHTS) was successfully launched on 23 September 2013, which enables the possibility of assessing temperature detection with the combined 118 GHz and 60 GHz oxygen bands (Gu et al.[15]).

The MWTS-II and MWHTS instruments, datasets and data pre-processing procedure are discussed, with the description of bias characteristics and results of the bias correction of the MWTS-II and MWHTS observed brightness temperatures described in section 2. Section 3 describes the retrieval algorithms, section 4 presents an optimization method based on the branch and bound algorithm, and calculates the radiometric information contents of the MWTS-II and MWHTS observations. Finally, the atmospheric temperature retrieval trials from each sounder, and then that combined from both sounders are presented in section 5, with conclusions given in section 6.

2 DESCRIPTION OF THE MICROWAVE HUMIDITY AND TEMPERATURE SOUNDER AND THE MICROWAVE TEMPERATURE SOUNDER–II

2.1 *Instrument characteristics*

The FY-3C satellite was successfully launched into a near-polar, circular, morning-configured (1005 local time) orbit at an altitude of 836 km above the Earth and an inclination angle of 98.75° to the equator. The MWHTS and MWTS-II instruments are part of the FY-3C satellite payloads, and are both designed using the total power radiometers technique (Gu et al. [15]; Bao [16]). The MWHTS instrument has eight temperature sounding channels at the 118.75 GHz oxygen absorption line, five humidity sounding channels at the 183 GHz water vapor absorption line, and two window channels at 89 GHz and 150 GHz. The MWTS-II instrument has 13 channels in the 60 GHz oxygen absorption band. Both sounders scan in a cross-track manner within ±53.35° with respect to the nadir direction, and complete one scan every 2.66 s. Each field of view (FOV) in the scan line corresponds to one scan angle. The MWHTS has a nominal FOV of 16 km at the nadir, and each scan line has 98 fields of view. The MWTS-II has a nominal FOV of 33 km at the nadir, and each scan line has 90 fields of view. The MWHTS and MWTS-II channel characteristics are listed in Tables 1 and 2, respectively. Fig.1 shows the weighting functions for the MWTS-II and MWHTS channels, which are calculated from a 1976 standard US atmospheric profile at nadir using the Millimeter-wave Propagation Model (MPM)-93 (Liebe et al.[17]).

The weighting functions indicate the relative contribution of each atmospheric layer to the observed brightness temperature (Karbou et al.[18]). Fig. 1a shows that MWHTS channels 2–9 detect the atmospheric temperature mainly in the stratosphere (from the surface to 30 hPa), while channels 11–15 detect the humidity in the troposphere. Fig. 1b shows that the MWTS-II channels 3–13 profile the atmospheric temperature from the surface to 3 hPa. In addition, the weighting functions for MWHTS channel 1 and 10 and MWTS-II channel 1 and 2 with frequencies near the atmospheric absorption window have their maximum closer to the surface. These channels are affected by the radiation from both the Earth's surface and the atmosphere and hence may be used to obtain surface information. The height distributions of the peak weighting functions of

the MWHTS and MWTS-II instruments are shown in Tables 1 and 2, respectively.

Table 1. MWHTS channel characteristics.

Channel	Frequency (GHz)	Sensitivity (K)	In-fight sensitivity (K)	Calibration accuracy (K)	Peak weighting function (hPa)
1	89.0	1.0	0.23	1.3	Window
2	118.75±0.08	3.6	1.62	2.0	30
3	118.75±0.2	2.0	0.75	2.0	50
4	118.75±0.3	1.6	0.59	2.0	100
5	118.75±0. 8	1.6	0.65	2.0	250
6	118.75±1.1	1.6	0.52	2.0	350
7	118.75±2.5	1.6	0.49	2.0	Surface
8	118.75±3.0	1.0	0.27	2.0	Surface
9	118.75±5.0	1.0	0.27	2.0	Surface
10	150.0	1.0	0.34	1.3	Window
11	183.31±1.0	1.0	0.47	1.3	350
12	183.31±1.8	1.0	0.34	1.3	450
13	183.31±3.0	1.0	0.30	1.3	550
14	183.31±4.5	1.0	0.22	1.3	750
15	183.31±7.0	1.0	0.27	1.3	850

Table 2. MWTS-II channel characteristics.

Channel	Frequency (GHz)	Sensitivity (K)	In-fight sensitivity (K)	Calibration accuracy (K)	Peak weighting function (hPa)
1	53.30	1.5	0.26	1.5	Window
2	51.760	0.9	0.20	1.5	Window
3	52.800	0.9	0.21	1.5	950
4	53.596	0.9	0.18	1.5	700
5	54.400	0.9	0.19	1.5	400
6	54.940	0.9	0.19	1.5	250
7	55.500	0.9	0.23	1.5	180
8	57.290(f0)	0.9	0.74	1.5	90
9	f_0±0.217	1.5	0.66	1.5	50
10	f_0±0.322±0.048	1.5	0.49	1.5	25
11	f_0±0.322±0.022	2.3	0.53	1.5	10
12	f_0±0.322±0.010	3.0	0.93	1.5	6
13	f_0±0.322±0.005	4.5	2.11	1.5	3

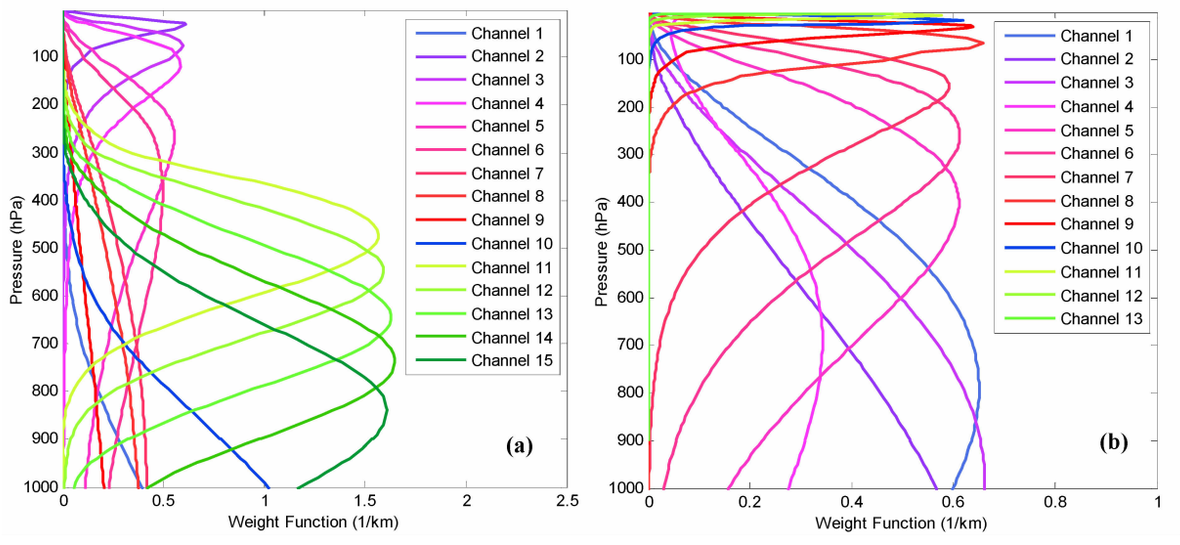

Figure 1. Weighting functions for the (a) MWHTS and (b) MWTS-II instruments.

2.2 *Data description and pre-processing*

The datasets used here include the following. (1) Level 1b MWTS-II and MWHTS brightness temperatures from the National Satellite Meteorological Center (NSMC) (http://www.nsmc.cma.gov.cn/). The MWTS-II and MWHTS measurements are both calibrated through a two-point calibration algorithm. The Level 1b brightness temperatures are converted from the instrument calibration data, including the radiometric counts from cold space and a warm target, the warm target temperature and instrument temperature. These calibration data are converted to brightness temperature using a non-linear correction, with the coefficient derived from the prelaunch thermal vacuum data, cross-polarization correction and correction of antenna spill-over effects. (2) European Centre for Medium Range Weather Forecasts (ECMWF) ERA Interim reanalysis dataset obtained from the ECMWF website (http://apps.ecmwf.int/datasets/), which is a global assimilation system including many sounding observations, such as radiosondes and in-situ sounders. The profile data comprise temperature, humidity and cloud liquid water on a total of 37 pressure levels unevenly spaced from 1–1,000 hPa. The surface data comprise surface pressure, skin temperature, 2 m temperature, 2 m dewpoint temperature, and the 10 m wind speed. The reanalysis dataset has a horizontal resolution of 1° × 1° and a temporal resolution of 6 h (i.e. with data available at 0000 UTC, 0600 UTC, 1200 UTC and 1800 UTC); (3) the National Centers for Environmental Prediction (NCEP) Global Forecast System (GFS) 6 h forecast dataset obtained from the NCEP website (http://rad.ucar.edu/datasets/) is produced by the Global Data Assimilation System (GDAS) and the Global Spectral Model (GSM) forecast system at NCEP. While the horizontal and temporal resolutions, profile parameters and the surface parameters of the NCEP forecast dataset are the same as that of the ECMWF reanalysis dataset, the profile data have a total of 26 pressure levels unevenly spaced from 10–1,000 hPa. Therefore, to match the number of pressure levels from the ECMWF reanalysis, the NCEP profiles are interpolated. Our datasets cover a geographic area of 180°W–180°E and 0°–30°N from 1 February to 30 June 2014. Data pre-processing includes initially generating collocated brightness temperatures, with the criteria for collocating MWHTS observations with MWTS-II observations that their time difference is less than 2 s and the absolute distance between their positions (latitude and longitude) is less than 0.1°. The criteria for collocating the brightness temperatures with climatological datasets (ECMWF reanalysis and NCEP forecast datasets) are that their time difference is less than 0.5 h and the absolute distance between their positions (latitude and longitude) is less than 0.5°. The simulation and bias correction of brightness temperatures in the collocated dataset are then carried out, with the brightness temperatures simulated by the Radiative Transfer for TOVS (RTTOV) model (Hocking et al. [19]). The bias of brightness temperatures are corrected by the neural network (NN) correction method (He et al. [20]). Finally, the collocated dataset from 1 February to 31 May 2014 is taken as the statistical analysis dataset with 17,396 collocated samples over land and 150,609 collocated samples over the ocean. The collocated dataset from 1 to 30 June 2014 is taken as the testing dataset with 2,692 collocated samples over land and 37,918 collocated samples over the ocean. The overall data pre-processing procedures and parameters are summarized in Fig.2 and Table 3, respectively.

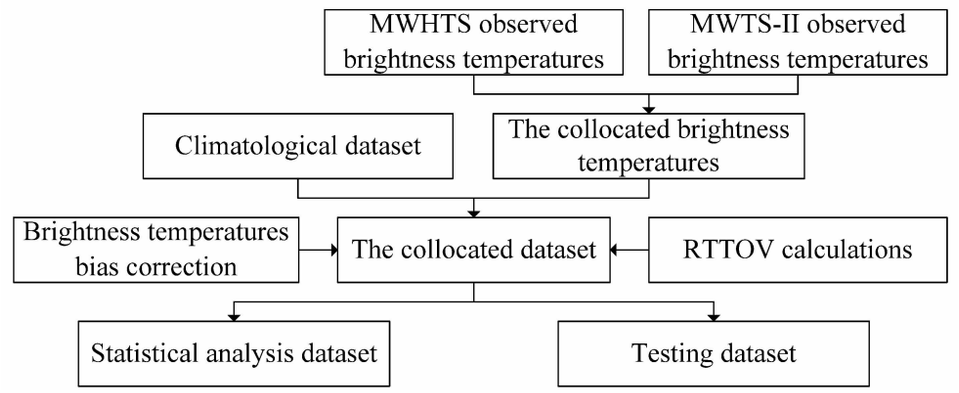

Figure 2. The flow chart for the data pre-processing procedure.

2.3 *Bias characteristics of observations*

While residual biases vary with the scan positions, where the observed brightness temperatures of the MWTS-II and MWHTS instruments have been scanned in a cross-track manner, the simulations from the RTTOV model take the scan angle of the instruments into account (Guo et al. [21]). We calculate the mean biases between the observations and simulations in the testing dataset, with the distributions of the mean biases at different scan positions shown in Fig.3.

Table 3. Brightness temperatures and atmospheric parameters in the collocated dataset.

Data source	Parameter
MWTSII/MWHTS	simulated brightness temperature observed brightness temperature corrected brightness temperature
ECMWF ERA Interim reanalysis	temperature profile, humidity profile cloud liquid water profile, surface pressure skin temperature, 2-m temperature 2-m dewpoint temperature, 10-m wind speed
NCEP GFS 6 h forecast	temperature profile, humidity profile cloud liquid water profile, surface pressure skin temperature, 2-m temperature 2-m dewpoint temperature, 10-m wind speed

Figure 3 shows that the biases of observed brightness temperatures from different channels of the MWTS-II and MWHTS temperature soundings vary greatly with scan angles, with significant differences between channels as they are located in different oxygen absorption bands, or in a different position of the same oxygen absorption band. Compared with the mean biases of observations in the MWHTS temperature sounding channels, the mean biases in the MWTS-II channels are negative and larger. However, the biases in the MWHTS temperature sounding channels vary significantly at the adjacent scan positions, though the bias values are small. In addition, it is worth noting that there is a dip in the bias in the first five scan positions for the MWHTS temperature sounding channels, implying a contamination at the initial scan positions. The actual sources of scanning biases in the MWTS-II and MWHTS channels may be a combination of some factors, such as solar contamination on the calibration target, frequency drift, and the non-linear correction in the calibration method. The root causes of these biases will be studied further. As these biases may adversely affect the accurate retrieval of the temperature, they should be corrected, especially for the physical retrieval algorithm. The observations of the testing dataset are corrected by the NN correction algorithm, with the results also shown in Fig.3. For the MWTS-II bias correction, Fig.3a shows that the mean biases of the corrected brightness temperatures approach zero. Except for the MWTS-II channels 3 –6, the angle dependencies of the bias are removed in the other channels. For the MWHTS bias correction, Fig.3b shows that the biases and the angle dependencies of the bias are smaller than that without the bias correction. In addition, the dips in bias in the first five scan positions have almost disappeared. To quantitatively describe the bias correction results, the root-mean-square errors (RMSE) of the observed brightness temperature bias before and after correction are shown in Fig.4.

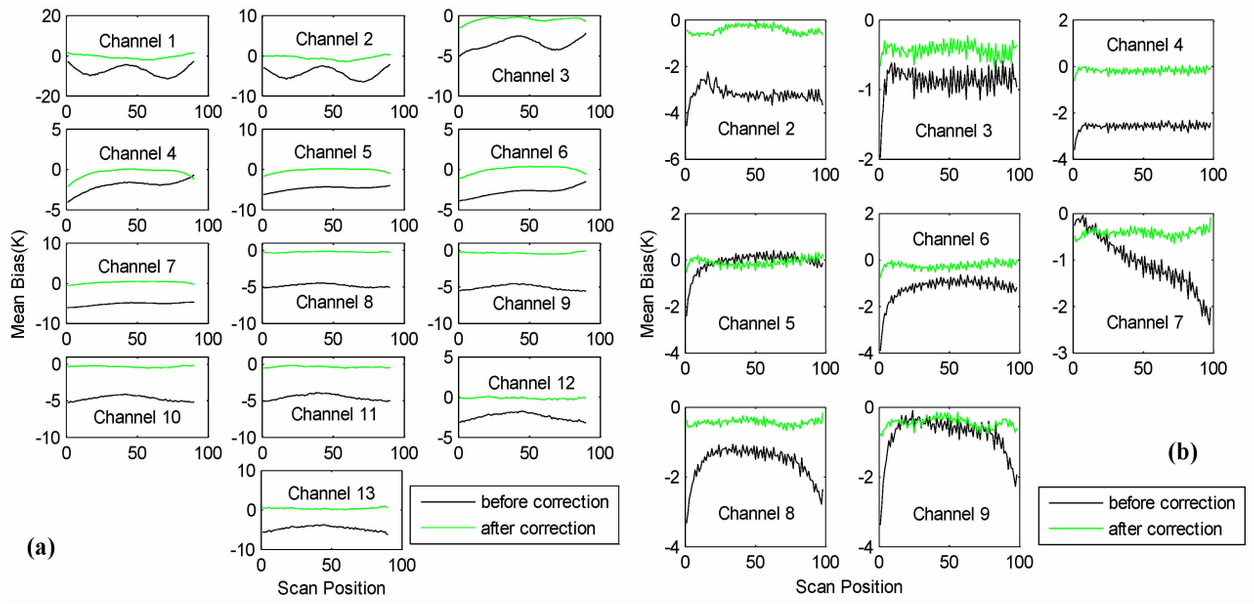

Figure 3. The mean biases and bias correction results of observed brightness temperatures. (a): MWTS-II; (b): MWHTS.

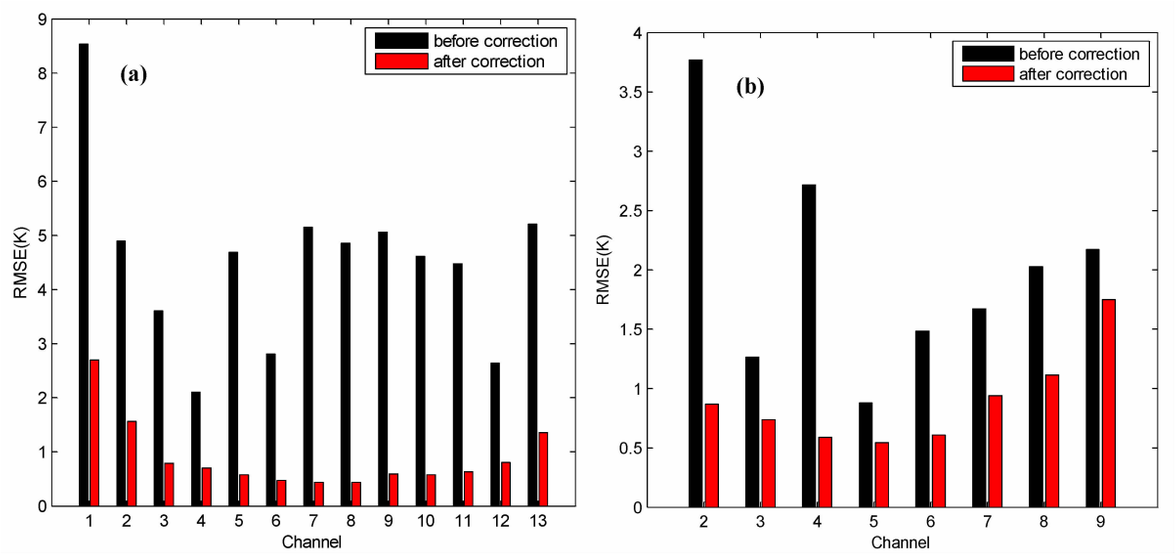

Figure 4. RMSE of the bias before and after bias correction for the (a) MWTS-II and (b) MWHTS observations.

Figure 4 shows that, before the bias correction, the RMSE of the bias for MWTS-II is significantly higher than that in the MWHTS temperature sounding channels, amounting to > 3 K, with the exception of the MWTS-II channels 4, 6 and 12, with > 8 K in channel 1 in particular. For the MWHTS channels, the RMSE of the bias in channel 2 is 3.8 K, and < 3 K in the other channels. After the bias correction, the RMSE of the bias in MWTS-II channels 1 and 2 and MWHTS channel 9 are 2.8 K, 1.5 K and 1.7 K, respectively, but the RMSE for the other channels is < 1 K. For the MWTS-II channels 1 and 2 and MWHTS channel 9, which are sensitive to surface disturbances, it is difficult to distinguish whether the radiometric contribution is from the surface or the atmosphere, implying a complex relationship between the atmospheric temperature and the bias of observations, which further degrades the performance of the correction method. Based on the above analysis, we find that, though the biases between the observations and simulations from the MWTS-II and MWHTS channels are large, they can be significantly reduced using the NN correction algorithm.

3 RETRIEVAL ALGORITHMS

Statistical and physical retrieval methods are used to retrieve the atmospheric temperature profiles. The NN and 1D-var algorithms are generally regarded as statistical and physical methods, respectively, with both able to represent the non-linear relationship between the satellite observations and atmospheric temperature.

3.1 *Neural networks retrieval algorithm*

Neural networks have recently been applied in the processing of remote sensing data, since they compute analytical relationships between highly complicated inputs and outputs. We focus on the backpropagation learning algorithm because of its powerful non-linear reflection ability and training functionality. Based on previous work in the application of NNs for the retrieval of atmospheric geophysical parameters, and also considering the non-linear nature of temperature retrieval, a three-layer backpropagation NN is selected, with the schematic diagram containing one hidden layer shown in Fig.5. The input layer, where no calculation is carried out, has L nodes representing the length of the input vector $\boldsymbol{X}$, with each node in the input layer connected to all M nodes in the hidden layer, which perform the non-linear computation and are connected to each node of the output layer. The output vector $\boldsymbol{Z}$ of length N is generated by a weighted sum over the output vector $\boldsymbol{Y}$ of the hidden layer. See Yao et al. [22] and Polyakov et al. [23] for additional details on the initialization, training, optimization and other advanced topics of NNs.

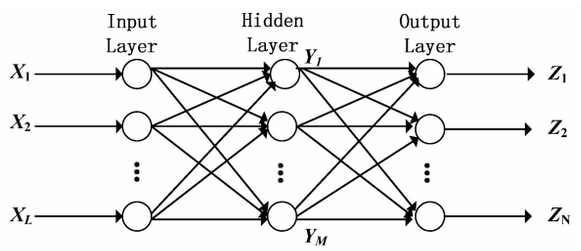

Figure 5. Diagram of the three-layer backpropagation NN.

The corrected brightness temperatures in the statistical analysis dataset are the input vector $\boldsymbol{X}_L$ of length L corresponding to the 13 and 8 observational channels for the MWTS-II and MWHTS instruments, respectively. The atmospheric temperature profiles are taken as the output vector $\boldsymbol{Z}_N$ of length N equal to the number of pressure levels of the profile data. The pairs of input/output vectors are used to train the NN, and the steepest descent method is selected for the training phase. Testing reveals that the optimal number of

hidden nodes in the hidden layer is 30 and 28 for the MWTS-II and MWHTS observations, respectively. Here, 90% of the pairs are used to determine the weights and biases in the NN, with the remaining 10% used to validate the training.

3.2 *One-dimensional variational retrieval algorithm*

3.2.1 ALGORITHM PRINCIPLE

The 1D-var retrieval algorithm is the typical representative of physical retrieval methods containing two main parts. One is the advanced radiative transfer model for calculating radiances and the gradient of radiance (or weighting function matrix), and the other is a scheme for minimizing the cost function, which weights the relative contributions of a priori information and satellite measurements (Liu and Weng[24]). Assuming errors in both satellite measurements and a priori information are neither biased nor correlated, and have Gaussian distributions, the best estimate of minimizes the cost function (Rodgers[25]).

$$J=\frac{1}{2}(\boldsymbol{x}-\boldsymbol{x}^b)^{\mathrm{T}}\boldsymbol{B}^{-1}(\boldsymbol{x}-\boldsymbol{x}^b)+\frac{1}{2}[\mathrm{H}(\boldsymbol{x})-\boldsymbol{I}]^{\mathrm{T}}\boldsymbol{R}^{-1}[\mathrm{H}(\boldsymbol{x})-\boldsymbol{I}] \quad (1)$$

where $\boldsymbol{x}^b$ is the background profile, $\boldsymbol{B}$ is the background covariance matrix, $\boldsymbol{R}$ is the observational error covariance matrix, which includes the forward model error and the instrument noise, H is the forward operator that calculates the brightness temperature simulations at the atmospheric state variable $\boldsymbol{x}$, $\boldsymbol{I}$ is the satellite observations, and T represents the matrix transpose. The minimum of the cost function is found from an iterative calculation of the descent direction at the state $\boldsymbol{x}$. The value of the cost function gradient at each iteration is derived as

$$\nabla_x J=\boldsymbol{B}^{-1}(\boldsymbol{x}-\boldsymbol{x}^b)+\boldsymbol{H}^{\mathrm{T}}(\boldsymbol{x})\boldsymbol{R}^{-1}[\mathrm{H}(\boldsymbol{x})-\boldsymbol{I}] \quad (2)$$

where $\boldsymbol{H}$ is the weighting function matrix. An optimal solution to (2) is obtained by setting the gradient of the cost function zero and is expressed as

$$\boldsymbol{x}_{n+1}=\boldsymbol{x}^b+\boldsymbol{B}\boldsymbol{H}^{\mathrm{T}}(\boldsymbol{x}_n)[\boldsymbol{H}(\boldsymbol{x}_n)\boldsymbol{B}\boldsymbol{H}^{\mathrm{T}}(\boldsymbol{x}_n)+\boldsymbol{R}]^{-1}[\boldsymbol{I}-\mathrm{H}(\boldsymbol{x}_n)-\boldsymbol{H}(\boldsymbol{x}_n)(\boldsymbol{x}^b-\boldsymbol{x}_n)] \quad (3)$$

where n is the iteration index, and the start point $\boldsymbol{x}_1$ of the iteration is the first guess.

3.2.2 ONE-DIMENSIONAL VARIATIONAL RETRIEVAL SYSTEM PARAMETERS

For the a priori information in the statistical analysis, the temperature profiles of the ECMWF reanalysis data are used to generate the background covariance matrix $\boldsymbol{B}$, which is calculated by the same method as that of He et al.[26]. To avoid the different effects on MWTS-II and MWHTS retrieval accuracy resulting from the first guess, the NCEP 6-h forecast temperature profiles are selected. In addition, the first guess is also taken as the background profile in our study.

For the bias $\mathrm{H}(\boldsymbol{x})-\boldsymbol{I}$, the NN correction algorithm is used. The NN structure, input vector and learning algorithm in the training phase are the same as that of the NN retrieval algorithm in section 3.1, but the output vector is replaced by the biases between observations and simulations. Based on many training tests, we find that the optimal numbers of hidden nodes in the hidden layer are 50 and 48 for the MWTS-II and MWHTS observations, respectively.

After correcting the observed brightness temperatures, the biases between the simulations and the corrected observations, as well as the sensitivities measured in flight (see Tables 1 and 2 for the MWHTS and MWTS-II instruments, respectively) are used to calculate the observational error covariance matrix $\boldsymbol{R}$. Both the observational error covariance matrix $\boldsymbol{R}$ as well as the quality control of observations, and the convergence criterion, are calculated using the same method as that of He et al.[27].

Based on the above analysis, the MWTS-II and MWHTS 1D-var retrieval systems are built to retrieve the atmospheric temperature profiles.

4 OPTIMIZATION OF THE CHANNEL COMBINATION

4.1 *Radiometric information content calculation*

In theory, the more information contained in the observations, the higher the retrieval accuracy obtained. The number of degrees of freedom DOF is selected as the quantitative index used to evaluate the radiometric information contents of observations, and is computed as the trace $\mathrm{tr}(\cdot)$ of the averaging kernel matrix, $\mathrm{DOF}=\mathrm{tr}(A)$ (Sahoo et al.[14]), where

$$\boldsymbol{A}=\boldsymbol{B}\boldsymbol{H}^T(\boldsymbol{H}\boldsymbol{B}\boldsymbol{H}^T+\boldsymbol{R})^{-1}\boldsymbol{H} \quad (4)$$

and $\boldsymbol{H}$ is the weighting function matrix, $\boldsymbol{B}$ and $\boldsymbol{R}$ are the background covariance matrix and observation error covariance matrix, respectively.

We focus on the channel combination, including the 13 channels of the MWTS-II observations and 8 temperature sounding channels of the MWHTS observations. However, according to the temperature weighting-function analysis, we find some channels in the channel combination have similar sensitivities to a certain atmospheric layer, such as the MWTS-II channel 6 and MWHTS channel 5, which means there is some redundant information in the channel combination.

4.2 *Optimization algorithm for the channel combination*

In general, to identify and remove the redundant elements of a large set, feature selection (i.e. variable selection) must be performed, requiring the selection of a subset of relevant variables from a larger set (Guyon and Elisseeff [28]; Ludwig and Nunes [29]). Here, the variables are the channels, and are sorted with a branch and bound algorithm (Narendra and Fukunage[30]).

Figure 6 shows the solution tree based on a branch and bound feature selection algorithm. The set $\boldsymbol{K}_m$ contains both redundant and relevant features, i.e., $\boldsymbol{k}_1$, $\boldsymbol{k}_2$, $\cdots\boldsymbol{k}_m$, where m is the number of elements of the set. To select a subset of n elements, $\boldsymbol{K}_n$ which are those n elements with the most relevant features within $\boldsymbol{K}_m$, the

selection criterion ξ is required. Any subset should have a value of ξ that is no larger than that of any proper superset when ξ is monotonic. However, removing a particular feature from a large set may not have a serious impact on the criterion values. Therefore, each feature in the m-feature set $\boldsymbol{K}_m$ is excluded (one at a time), and the criterion value of ξ is calculated for each of the subsets at level 1 in Fig.6. The subset having the maximum value of ξ ($\boldsymbol{K}_{m-1}$) is selected, and then all other subsets are abandoned. All subsets of $\boldsymbol{K}_{m-1}$ at level 2 have a value of ξ which is not larger than that of $\boldsymbol{K}_{m-1}$. The subset of $\boldsymbol{K}_{m-1}$, which has the maximum value of ξ ($\boldsymbol{K}_{m-2}$), is selected, and the others are abandoned. This process of selecting the subset with the maximum value of ξ, and then abandoning all others is repeated until the desired number of variables is attained.

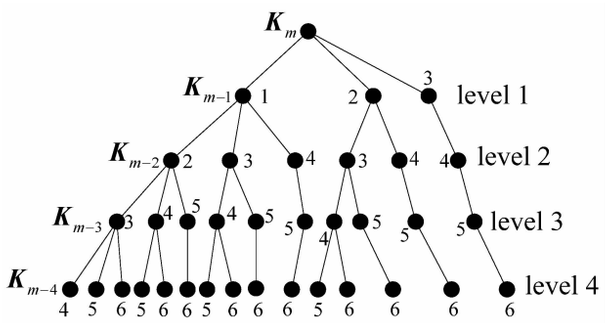

Figure 6. Solution tree based on a branch and bound feature selection algorithm.

Here, the channel combination described in section 4.2 is taken as the set $\boldsymbol{K}_m$, where the features are the weighting functions corresponding to the different channels, and the value of m is 21. The DOF for the channel combination is taken as the selection criterion. The optimized combination generated by the branch and bound algorithm is $\boldsymbol{K}_n$. Considering that the peak weighting-function heights of MWTS-II are distributed throughout the entire atmosphere, the desired number of features n is equal to that of the MWTS-II channels. Therefore, over both land and ocean, we obtain the optimized combinations containing the MWTS-II channels 3–13 and the MWHTS channels 8 and 9.

4.3 *Radiometric information content analysis*

The DOF of the measurements from MWTS-II channels 1–13 and MWHTS channels 2–9, the channel combination and the optimized combination is calculated. The parameters required for the averaging kernel in (4), i.e., the weighting function matrix $\boldsymbol{H}$, the background covariance matrix $\boldsymbol{B}$ and the observation error covariance matrix $\boldsymbol{R}$ are calculated by the same method as that in (3). The mean temperature profile in the statistical analysis is used to calculate the weighting functions, since its calculation is greatly affected by the atmospheric conditions. Table 4 lists the DOF of the observations over land and ocean.

Table 4. The DOF over land and ocean for different channel combinations.

Channel	DOF	
	over land	Over ocean
MWHTS	3.8601	4.0039
MWTS-II	6.2943	6.5315
MWTS-II+ MWHTS	6.6373	7.0305
Channel optimization	6.5308	6.8681

Table 4 shows that the DOF for the MWTS-II observations is higher than that of the MWHTS observations, possibly because their temperature sounding channels are located in different oxygen absorption bands, and the number of channels is different. The DOF for the observations over ocean is higher than that over land, probably because the simulated accuracy of the ocean-surface emissivity is always higher than that of land. The DOF of the channel combination is highest, however, since redundant information exists in the observations from the channel combination. Actually, the optimized combination is the improved MWTS-II channels in which channels 1 and 2 are replaced by MWHTS channels 8 and 9. The DOF of the optimized combination is higher than that of the MWTS-II channels alone. In theory, the more information contained in the observation, the higher the retrieval accuracy obtained. Therefore, for the retrieval of atmospheric temperature, from a theoretical point of view, we speculate that the retrieval accuracy of MWTS-II is higher than that of MWHTS, the retrieval accuracy of the optimized combination is higher than that of MWTS-II, with the channel combination having the highest retrieval accuracy.

5 COMPARISON OF RETRIEVAL RESULTS

The inversion of observations into atmospheric temperature profiles, including the corrected brightness temperatures obtained from the MWTS-II and MWHTS data in the testing dataset, is conducted using the NN and 1D-var algorithms. The bias and RMSE quantify the validation of the retrieval results based on ECMWF reanalysis data, which is used as the truth. According to the weighting-function analysis of the MWTS-II and MWHTS observations, we validate the temperature retrievals at pressure levels from 10–1,000 hPa.

5.1 *Retrieval results of the neural network algorithm*

The corrected brightness temperatures of the MWTS-II and MWHTS observations are calculated individually as inputs of the NN retrieval algorithm, with outputs being the temperature retrievals shown in Fig.7.

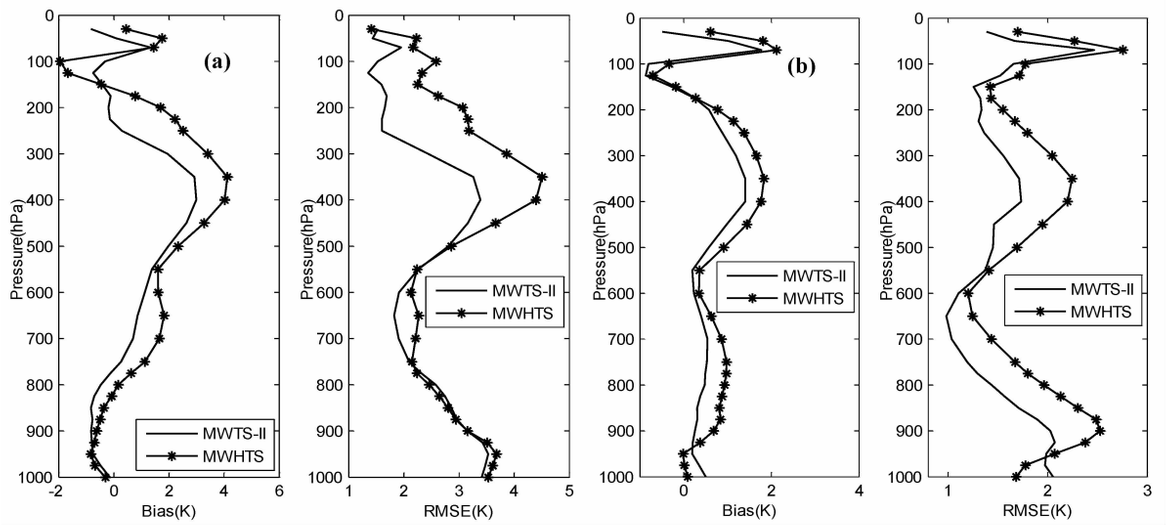

Figure 7. Comparison of temperature retrievals using the NN algorithm over (a) land and (b) the ocean.

Over land, Fig.7a shows that the bias for the MWTS-II retrieval is smaller than that of the MWHTS retrieval, except for the pressure levels around 100 hPa and 800 hPa. The accuracy for the MWTS-II retrieval is similar to that of the MWHTS retrieval at levels from 775–1,000 hPa and 500–550 hPa, while the other levels of the MWTS-II accuracy exceeds that of the MWHTS observations. Over the ocean, Fig.7b shows that the bias and RMSE of the MWTS-II retrieval are both smaller than that of the MWHTS retrieval at levels from 10–950 hPa, and compared with the retrievals over land, have a higher accuracy. Besides the different samples over land and ocean in the statistical analysis dataset, which can affect the trained results of the NN, the main cause of the different accuracies over land and ocean is possibly related to the surface emissivity, where the calculation of the land-surface emissivity is complicated, and the accuracy is always lower than that of the ocean-surface emissivity. In addition, the land surface has higher emissivity, making it difficult to distinguish the radiation from the surface and that from the atmosphere close to the surface, which is true for both the MWTS-II and MWHTS observations. According to the comparison of the retrieval results over land and ocean, we find that the MWHTS retrieval has a superior detection ability of temperature at the levels from 950–1,000 hPa, which opens up the possibility of improving the MWTS-II retrieval accuracy of temperature profiles in the atmospheric surface layer using the MWHTS observations. Based on the comparison of the retrieval results using the NN algorithm, it can be seen that the MWTS-II retrievals attain a higher accuracy than that of the MWHTS retrievals, which is consistent with the conclusion from the information content analysis in section 4.3.

5.2 *Retrieval results of the one–dimensional variational algorithm*

The 1D-var retrieval system is applied to the MWTS- II and MWHTS corrected brightness temperatures to estimate the atmospheric temperature profiles. In our retrieval system, the number of iterative times is generally less than five. Quality control of the MWTS-II retrieval results in a convergence of more than 95.4% and 96.1% of the solutions over the land and ocean, respectively. For the MWTS-II retrievals, more than 95.4% and 96.2% of solutions converge over land and ocean, respectively. The retrieval validation results are shown in Fig. 8.

Over land, Fig. 8a shows that the bias of the MWTS-II retrieval exceeds that of MWHTS retrieval, except at the levels from 10–100 hPa and 900–1,000 hPa. The accuracy of the MWHTS retrieval is higher than that of the MWTS-II retrieval at the levels from 500–1,000 hPa and 175–300 hPa, and is lower than that of MWTS-II retrieval at the levels from 300–450 hPa. The MWHTS retrievals are nearly equivalent to that of MWTS-II at the other levels. Over the ocean, Fig. 8b shows a larger bias of the MWTS-II retrieval than that of MWHTS retrieval at almost all pressure levels. The accuracy of the MWHTS retrieval is similar to that of the MWTS-II retrieval at the levels from 850–1,000 hPa, is higher than that of MWTS-II retrieval at the levels from 650–850 hPa and 125–300 hPa, and lower than that of the MWTS-II retrieval at the other levels. As for the results of the NN algorithm, the retrieval accuracy over the ocean is higher than that over the land. Retrieval results using the 1D-var algorithm are not consistent with the conclusion from the information content analysis in section 4.3, with the reason being that the physical retrieval method is affected by many factors, such as the background profiles, the background covariance matrix, the observation error covariance matrix, and the bias correction results.

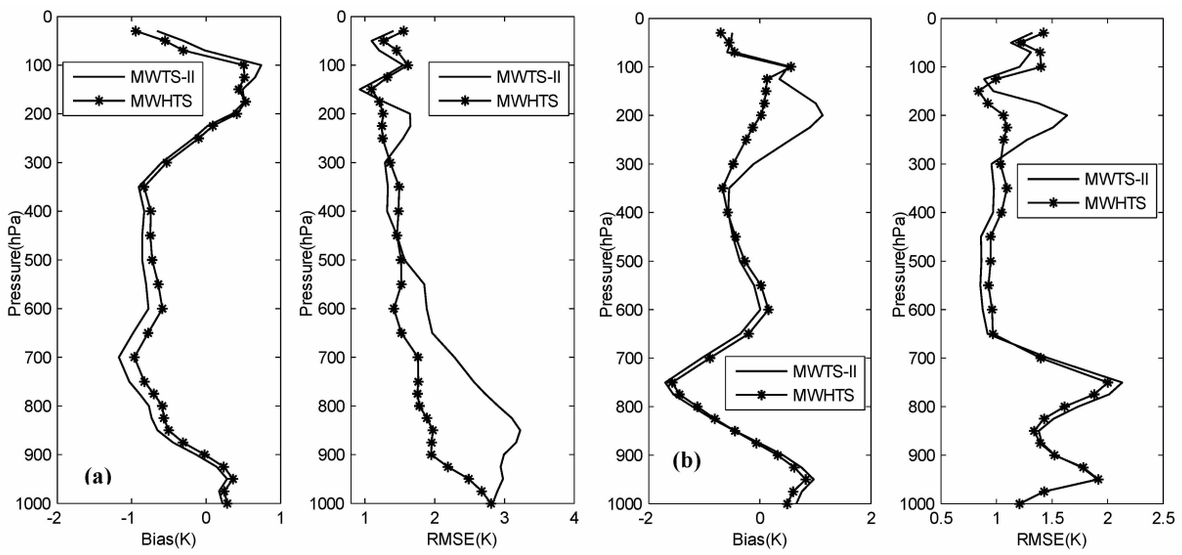

Figure 8. Results of temperature retrievals using the 1D-var algorithm over (a) land and (b) ocean.

Based on the above comparison of retrieval results using the NN and 1D-var retrieval algorithms, we elect to use the NN algorithm, whose retrieval results are consistent with the information content analysis, to validate the retrieval performance of the channel combinations, as well as the optimal channel combination.

5.3 *Retrieval results of the channel combination*

The corrected brightness temperatures of the channel and optimal combinations are considered individually as the input vector of the NN retrieval algorithm, which is again trained to retrieve the atmospheric profiles using the corresponding corrected brightness temperatures. Fig.9 shows the retrieval validation results.

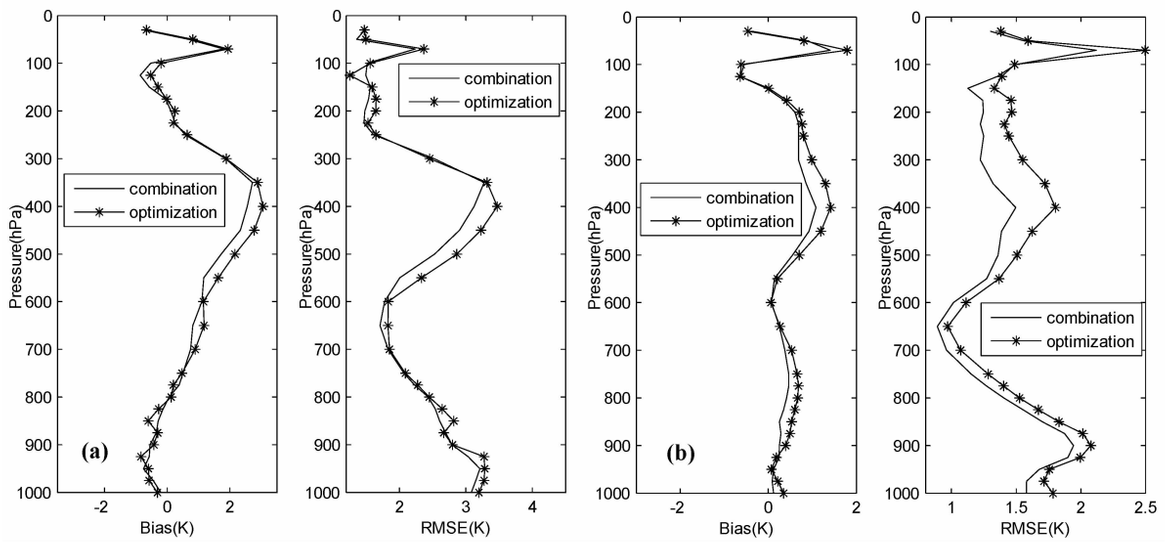

Figure 9. Results of retrievals using a channel combination and optimization over (a) land and (b) the ocean.

Over land, Fig.9a shows that the retrieval bias and RMSE of the channel combination are smaller than that of the optimized combination at the levels from 900–1,000 hPa and 350–700 hPa, with the retrieval accuracies similar at the other levels. Over the ocean, Fig.9b shows that the retrieval results of the channel combination are superior to that of the optimized combination at all pressure levels. Comparing these results with those from the MWTS-II and MWHTS retrievals individually, i.e., comparing Figs.9 with 7, we find improved results within the atmospheric surface layer with use of the optimal combination, which validates the presumption presented in section 5.1, but with similar retrieval accuracies at the other pressure

levels. In addition, the channel combination attains the highest retrieval accuracy, with the accuracy of the MWHTS retrieval being the worst of the four retrievals. The comparison of retrieval results using the NN algorithm proves the validity of the theoretical deduction of the radiometric information content analysis.

6 CONCLUSIONS

To evaluate the detection ability of the atmospheric temperature of the 60 GHz oxygen absorption band and the 118.75 GHz oxygen absorption line, we focus on the observed brightness temperatures collected by the MWTS-II and MWHTS instruments. The radiometric information contents of the MWTS-II channels 1–13 and the MWHTS temperature sounding channels 2–9 are calculated, and the atmospheric temperature profiles are retrieved using NN and 1D-var algorithms. Results with the NN algorithm show a higher accuracy of MWTS-II retrievals than that of the MWHTS retrievals, which agrees with results from the analysis of the radiometric information content. However, the results using the 1D-var algorithm show that MWTS-II and MWHTS retrievals have different strengths in certain atmospheric layers. For the NN algorithm, based on the comparison of the results of the MWTS-II and MWHTS retrievals, an optimal combination, including MWTS-II channels 3–13 and MWHTS channels 8–9, is suggested to improve the retrieval of atmospheric temperature profiles and the reproduction of atmospheric temperature near the surface layer.

The MWTS and MWHTS observed brightness temperatures, which are based on the 60 GHz and 118.75 GHz oxygen absorption band and line, respectively, are used to carry out the retrieval of atmospheric temperature profiles. However, compared with the MWHTS temperature sounding channels located in the 118.75 GHz oxygen absorption line, the number of MWTS-II channels located in the 60 GHz oxygen absorption band is different. In addition, the distributions of the peak weighting-function height and the weighting-function shape of the MWHTS and MWTS-II observations are also very different. These factors affect the evaluation of the 60 GHz and 118.75 GHz observations. Therefore, for the MWTS-II and MWHTS temperature sounding channels, selecting the similar weighting-function distributions and the same number of channels to further evaluate the detection ability of atmospheric temperature is the topic of future work.

Acknowledgement: The authors would like to thank NSMC for providing the MWTS-II and MWHTS brightness temperature data, as well as ECMWF and NCEP for providing climatological datasets.

REFERENCES:

[1] AHN M H, KIM M J, CHUNG Chu-yong, et al. Operational implementation of the ATOVS processing procedure in KMA and its validation [J]. Adv Atmos Sci, 2003, 20(3): 398-414.

[2] STAHLI O, MURK A, KAMPFER N, et al. Microwave radiometer to retrieve temperature profiles from the surface to the stratopause [J]. Atmos Measure Technol, 2013, 6(9): 2477-2494.

[3] EBELL K, ORLANDI E, HUNERBEIN A, et al. Combining ground-based with satellite-based measurements in the atmospheric state retrieval: Assessment of the information content [J]. J Geophys Res: Atmos, 2013, 118(13): 6940-6956.

[4] SMITH E W. Absorption and dispersion in the O_2 microwave spectrum at atmospheric pressures [J]. J Chem Phys, 1981, 74(12): 6658-6673.

[5] ROSENKRANZ P W. Interference coefficients for overlapping oxygen lines in air [J]. J Quantit Spectr Radiat Trans, 1988, 39(4): 287-297.

[6] WENG Fu-zhong, ZHAO Li-ming, FERRARO R R, et al. Advanced microwave sounding unit cloud and precipitation algorithms [J]. Radio Sci, 2003, 38(4): 1-13.

[7] FERRARO R R, WENG F, GRODY N C, et al. NOAA operational hydrological products derived from the Advanced Microwave Sounding Unit [J]. IEEE Trans Geosci Remote Sensing, 2005, 43(5): 1036-1049.

[8] BOUKABARA S A, GARRETT K, CHEN W, et al. MIRS: An all-weather 1DVAR satellite data assimilation and retrieval system [J]. IEEE Trans Geosci Remote Sensing, 2011, 49(9): 3249-3272.

[9] WEINMAN J A. The effect of cirrus clouds on 118 GHz brightness temperature [J]. J Geophys Res: Atmos, 1988, 93(D9): 11059-11062.

[10] GASIEWSKI A J, STAELIN D H. Statistical precipitation cell parameter estimation using passive 118 GHz O2 observations [J]. J Geophys Res: Atmos, 1989, 94(D5): 18367-18378.

[11] GASIEWSKI A J, BARRETT J W, BONANNI P G, et al. Aircraft-based radiometric imaging of tropospheric temperature and precipitation using the 118.75 GHz oxygen resonance [J]. J Appl Meteor, 1990, 29 (7): 620-632.

[12] GASIEWSKI A J, JOHNSON J T. Statistical temperature profile retrievals in clear air using passive 118 GHz O2 observations [J]. IEEE Trans Geosci Remote Sensing, 1993, 31(1): 106-115.

[13] GUO Yang, LU Nai-meng, Gu Song-yan. Simulation of the radiometric characteristics of 118 GHz and 183 GHz channels for FY-3C new microwave radiometer sounder [J]. J Infrared Millim Wave, 2014, 33 (5): 481-491 (in Chinese).

[14] SAHOO S, BOSCH-LIUIS X, REISING S C, et al. Radiometric information content for water vapor and temperature profiling in clear skies between 10 and 200 GHz [J]. IEEE J Sel Topics Appl Earth Observ Remote Sensing, 2015, 8(2): 859-871.

[15] GU Song-yang, GUO Yang, YOU Ran, et al. The performance of microwave sounders board on FY-3C satellite [J]. Adv Meteor Sci Technol, 2016, 6(1): 76-82 (in Chinese).

[16] BAO Jing-hua. The principle of FY-3C satellite microwave humidity and temperature sounder and preliminary analysis on its in-orbit performance [D]. Beijing: Chinese Academy of Science, 2014 (in Chinese).
[17] LIEBE H J, HUFFORD G A, COTTON M G. Propagation modeling of moist air and suspended water/ice particles at frequencies below 1000 GHz [C]. In proceedings of the AGARD 52nd Specialists Meeting of Electromagnetic Wave Propagation Panel, Palma De Mallorca, Spain, 17-21 May 1993.
[18] KARBOU F, AIRES F, PRIGENT C, EYMARD L. Potential of Advanced Microwave Sounding Unit-A (AMSU-A) and AMSU-B measurements for atmospheric temperature and humidity profiling over land [J]. J Geophys Res: Atmos, 2005, 110(D7).
[19] HOCKING J, RAYER P, RUNDLE D et al. RTTOV v11 users guide [R]. NWP-SAF report, Met Office, UK.
[20] HE Qiu-rui, WANG Zhen-zhan, HE Jie-ying. Bias correction for retrieval of atmospheric parameters from the Microwave Humidity and Temperature Sounder onboard the Fengyun-3C satellite [J]. Atmos, 2016, 7 (12): 1-20.
[21] GUO Yang, LU Nai-meng, QI Cheng-li, et al. Calibration and validation of microwave humidity and temperature sounder onboard FY-3C satellite [J]. Chin J Geophys, 2015, 58(1): 20-31 (in Chinese).
[22] YAO Zhi-gang, CHEN Hong-bin, LIN Long-fu. Retrieving atmospheric temperature profiles from AMSU-A data with neural networks [J]. Adv Atmos Sci, 2005, 22(4): 606-616.
[23] POLYAKOV A, TIMOFEYEV Y M, VIROLAINEN Y. Comparison of different techniques in atmospheric temperature-humidity sensing from space [J]. Int J Remote Sensing, 2014, 35(15): 5899-5912.
[24] LIU Quan-hua, WENG Fu-zhong. One-dimensional variational retrieval algorithm of temperature, water vapor, and cloud water profiles from advanced microwave sounding unit (AMSU) [J]. IEEE Trans Geosci Remote Sensing, 2005, 43(5): 1087-1095.
[25] RODGERS C D. Retrieval of atmospheric temperature and composition from remote measurements of thermal radiation [J]. Rev Geophys Space Phys, 1976, 14 (4): 609-624.
[26] HE Qiu-rui, WANG Zhen-zhan, HE Jie-ying. Inversion of the clear atmospheric temperature and humidity profiles based on FY-3C/MWHTS measurements [J]. Chin J Radio Sci, 2016, 31(4): 772-778 (in Chinese).
[27] HE Qiu-rui, WANG Zhen-zhan, HE Jie-ying. Retrieval of clear sky temperature and humidity profiles over land using measurements of FY-3C/MWHTS [J]. J Remote Sensing, 21(1): 27-39 (in Chinese).
[28] GUYON I, ELISSEEFF A. An introduction to variable and feature selection [J]. J Machine Learning Res, 2003, 3: 1157-1182.
[29] LUDWIG O, NUNES U. Novel maximum margin training algorithms for supervised neural networks [J]. IEEE Trans Networks, 2010, 21(6): 972-984.
[30] NARENDRA P M, FUKUNAGE K. A branch and bound algorithm for feature subset selection [J]. IEEE Trans Comput, 1977, 26(9): 917-922.

Citation: HE Qiu-rui, WANG Zhen-zhan, HE Jie-ying, et al. A comparison of the retrieval of atmospheric temperature profiles using observations of the 60 ghz and 118.75 ghz absorption lines [J]. J Trop Meteor, 2018, 24(2): 151-162.